Agricultural and Forest Meteorology 213 (2015) 126–137

Contents lists available at ScienceDirect

Agricultural and Forest Meteorology

journal homepage: www.elsevier.com/locate/agrformet

Passive microwave and optical index approaches for estimating surface conductance and evapotranspiration in forest ecosystems

Verónica Barraza[a,*], Natalia Restrepo-Coupe[b], Alfredo Huete[b], Francisco Grings[a], Eva Van Gorsel[c]

[a] Instituto de Astronomía y Física del Espacio (IAFE, CONICET-UBA), Pabellon IAFE, CABA, Buenos Aires, Argentina
[b] Plant Functional Biology and Climate Change Cluster (C3), University of Technology Sydney (UTS), Broadway, NSW 2007, Australia
[c] CSIRO Oceans and Atmosphere Flagship, Canberra, ACT, Australia

ARTICLE INFO

Article history:
Received 2 March 2015
Received in revised form 19 June 2015
Accepted 28 June 2015
Available online 9 July 2015

Keywords:
Microwave index
Optical indices
Evapotranspiration
Surface conductance

ABSTRACT

In this study, we evaluated and compared optical and passive microwave index based retrievals of surface conductance (Gs) and evapotranspiration (ET) following the Penman–Monteith (PM) approach. The methodology was evaluated over the growing season at five FLUXNET sites in the USA and Australia encompassing three forest types, deciduous broadleaf forest (DBF), evergreen needleleaf forest (ENF) and evergreen broadleaf forest (EBF). A subset of Gs values were regressed against individual and combined indices of NDWI, EVI, and FI (microwave frequency index), and used to parameterize the PM equation for retrievals of ET (PM-Gs). For this purpose, we used MODIS (MYD09A1) and AMSR-E passive microwave data to compute the VIs. Model performance was quantitatively evaluated through comparative analysis of the regression coefficients (r^2), and root mean square errors (RMSE). All indices correlated well with Gs over deciduous broadleaf forests, explaining 40–60% of Gs variations, however, the optical-based models had lower RMSE than the microwave FI model. In contrast, the FI model yielded the best performance to estimate Gs in evergreen forests (EBF and ENF). Overall, a combined microwave-optical model resulted in the best Gs estimates in these evergreen forests compared with the individual model approaches. In general, the PM-models explained more than 70% of the variance in LE with RMSE lower than 20 W/m^2. Based on these results, we developed a new approach combining optical and passive microwave indices based on their spatial vs. temporal synergies to generate Gs time series. This combined optical-microwave approach produced the best ET estimates for evergreen forest and offered a robust approach for deciduous forest without sacrificing precision.

1. Introduction

The ability to monitor evapotranspiration (ET) from the land surface is relevant for several applications requiring spatially-resolved estimates of moisture availability over large areas (Cleugh et al., 2007; Dodds et al., 2005; Meyer and Wayne, 1999). Remote sensing cannot measure surface turbulent flux exchanges directly; however various methods have been developed using parameterization techniques that vary from purely empirical to more physically based approaches based on the energy balance equation and using vegetation indices (VI) (Yebra et al., 2013) and land surface temperature (LST) (Cleugh et al., 2007; Kalma et al., 2008; Moran and Jackson, 1991).

Among these models, the Penman–Monteith (PM) equation (Allen et al., 1998; Monteith, 1985) is widely used. Cleugh et al. (2007) and Mu (2007) showed that the PM equation is a biophysically sound and robust framework for estimating daily ET at regional to global scales using remotely sensed data. ET estimations from remote sensing data are generally based on parameterizations of PM equation, which rely on the estimation of surface or canopy conductance using measurements at visible (VIS), near-infrared (NIR) and shortwave-infrared (SWIR) wavelengths (Glenn et al., 2011, 2010; Leuning et al., 2008; Yebra et al., 2013). The relation between canopy conductance and optical indices were analyzed by several authors (Grant, 1987; Guerschman et al., 2009; Matsumoto et al., 2005; Yebra et al., 2013).

Methods based on VI have been found useful as a monitoring tool for ecosystem water use (Glenn et al., 2010). Applications in water resource management require ET information over a range of temporal and spatial resolutions, from hourly to monthly time steps

* Corresponding author.
E-mail address: vbarraza@iafe.uba.ar (V. Barraza).

http://dx.doi.org/10.1016/j.agrformet.2015.06.020
0168-1923/

and from field to global scales. Unfortunately, no single satellite system affords global coverage at both high spatial and temporal resolution. So, methods are needed for combining information at different wavelengths and spatial and temporal resolutions. A higher spatial resolution can be achieved by Landsat (30–60 m), but the frequency (16 days) is a limiting factor for several applications. MODIS products provide information at 250 m, 500 m and 1 km with a temporal resolution between 1 and 16 days, however such optical data are severely limited by their sensitivity to clouds and aerosols. In contrast, passive microwave sensors, although at coarser spatial resolutions, have best temporal resolution (1–3 days) and less sensitivity to atmospheric conditions and thus can be useful in larger scale ecosystem monitoring applications.

In principle, microwave emissivity (defined as the ratio between brightness temperature and physical temperature measured at microwave frequencies) is complex and dependent on both vegetation and soil properties (moisture and structure). However, over forest ecosystems, where vegetation biomass is moderate to high, the canopy contribution is dominant and the microwave signal becomes sensitive mainly to vegetation moisture and structure (Barraza et al., 2014a; Ferrazzoli and Guerriero, 1996; Min and Lin, 2006). Based on this relation, Min and Lin (2006) found that microwave indices, such as the Emissivity Difference Vegetation Index (EDVI) were empirically sensitive to the evapotranspiration and evapotranspiration fraction. Moreover, experimental work by Li et al. (2009) found that fast changes of EDVI represents canopy responses to changes of environmental conditions, such as vapor pressure deficit (VPD), water potential and CO_2 concentration, the same variables that determine canopy resistance.

In an earlier study we evaluated vegetation and soil properties that influence the microwave frequency index (FI) (Barraza et al., 2014a) over different ecosystems. Among other results, we found that day to day changes in FI (canopy scattering properties) computed at vertical polarization, using Ka and X bands, for areas with relatively high leaf area index (LAI) were sensitive to canopy moisture and changes in LAI (LAI > 2). It has also been found that changes in canopy (leaves + stems) water content can be monitored using FI at LAI > 2 ecosystems (Barraza et al., 2014a). Since stomata conductance is closely related to canopy moisture (Goldstein et al., 2008, 1998; Pfautsch et al., 2010; Zhang et al., 2013) and structure ((Jarvis and McNaughton, 1986)), we foresee an indirect link between surface conductance (Gs) and FI.

Several studies have been undertaken to relate microwave indices with ET (Jones et al., 2012; Li et al., 2009; Min and Lin, 2006), but there are few studies involving multiyear datasets and no direct attempt to estimate ET based on passive microwave and optical data over different forest ecosystems. New studies that use a synergy of sensors (microwave and optical) might be useful to improve the characterization of land surface conditions at appropriate temporal and spatial scales and thus help to support regional climate modeling applications (Pipunic et al., 2013).

In this work, our aim is to improve satellite-based ET retrievals by combining passive microwave and optical vegetation indices using the Penman–Monteith approach. We assessed individual approaches and combined synergies among the indices over different forest ecosystems in USA and Australia. The objectives were: (1) to assess the capability of microwave and optical indices to estimate Gs and ET; (2) to quantify ET with the PM equation using Gs estimations and meteorological data; (3) to compare both approaches (optical and microwave) and evaluate the error for Gs and ET estimations independently, (4) to address the eddy covariance-remote sensing footprint issues by comparing ET obtained at different scales with in-situ observations, and (5) to propose new models based on the combination of optical and microwave indices.

2. Methodology

2.1. Satellite microwave and optical vegetation indices data set

We used the Frequency Index (FI) (Ferrazzoli and Guerriero, 1996) for our analyses, calculated using the brightness temperatures measured at 37 GHz (Ka Band) and 10.6 GHz (X band) (Paloscia and Pampaloni, 1988) obtained from Advanced Microwave Scanning Radiometer – EOS (AMSR-E/AQUA) (Kawanishi et al., 2003) in ascending overpasses from 2002 to 2006. In Paloscia and Pampaloni (1992) and Barraza et al. (2014a) it was shown that one can monitor plant water status using the FI computed at these frequencies. We used FI calculated at vertical rather than horizontal polarization since this yields a higher correlation with vegetation state properties (Min and Lin, 2006). It was shown that for regions in which vegetation biomass is moderate to high, FI depends mostly on canopy condition (Ferrazzoli and Guerriero, 1996). Therefore, in the above-mentioned cases, FI becomes a function of canopy structure (i.e. leaves and stems geometry) and canopy moisture content (i.e., leaves and stems moisture content). Other passive microwave indices, like the polarization index, are less sensitive to vegetation moisture (Barraza et al., 2014a), and therefore not suitable for this application.

The differential sensitivity of microwave indices to (i) vegetation moisture (Barraza et al., 2014b; Ferrazzoli et al., 1992; Min and Lin, 2006) and (ii) soil moisture (Jackson, 1997) depend on the frequency of the passive microwave sensor and the key geometrical and dielectric characteristics of the land cover. In spite of this, different passive microwave indices, which are mainly sensitive to i or ii, could be applied for ET analysis. However, this sensitivity will define the type of relation between these indices and ET (Barraza et al., 2014a). Moreover, passive microwave indices sensitive to vegetation moisture, canopy structure and biomass changes have been applied for vegetation phenology analysis (Andela et al., 2013; Jones et al., 2012; Min and Lin, 2006), vegetation drought response (Frolking et al., 2011), potential growing season variability (Kimball et al., 2006) and seasonal changes in canopy CO_2 exchange (Min and Lin, 2006).

FI is influenced by land surface properties, such as vegetation, soil and snow. During the growing season, FI variations are generally related to vegetation properties. We excluded snow conditions using air temperature (Ta), obtained from meteorological stations, when Ta < 5 °C as a proxy to remove dormant season and snow periods. In this study, observations during precipitation events were excluded from the analysis with the aid of in situ precipitation data. The emission is strongly affected by the presence of rainfall during an acquisition, due to the important contribution of cold raindrops to the overall emissivity. As we calculated 8-day composite periods of FI (to align with MODIS time series composite criteria), we expect that using these methodology the uncertainties associated with precipitation to be negligible.

Yebra et al. (2013) found that no single Moderate Resolution Imaging Spectroradiometer (MODIS) optical vegetation index (VI) showed the best performance to estimate ET and Gs over all land cover types analyzed. We computed two MODIS satellite VIs (Table 2): the normalized difference water index (NDWI), a canopy moisture-based vegetation index and the enhanced vegetation index (EVI), as a chlorophyll-based greenness index, using the 8-day Aqua-MODIS land surface reflectance product (MYD09A1) with 500 m of spatial resolution from 2002 to 2006. Using the quality assessment (QA), information provided in this product, lower quality data and data with partial or complete cloud cover were removed from the analysis. The quality flags used were: MODLAND QA bits (ideal quality – all bands), atm. corr. Performed (yes), cloud state (clear) and cirrus detected (none). The VI products were aggregated to two different spatial scales, 1 km and also 25 km in order

to match the AMSR-E footprint from the same Aqua platform and 13.30 h overpass time. As the tower flux footprint is only a small fraction of the AMSR-E footprint, scale inconsistencies may have a certain effect on the evaluation of eddy covariance flux tower and passive microwave indices, and for this reason, we conducted our analyses using MODIS VIs at two different spatial resolutions.

AMSR-E data was downloaded from the National Aeronautics and Space Administration (NASA) data depository (http://reverb.echo.nasa.gov/). MODIS data was downloaded from Oak Ridge National Laboratory Distributed Active Archive Center (ORNL DAAC), MODIS subset land products, Collection 5. Available on-line (http://daac.ornl.gov/MODIS/modis.html) from ORNL DAAC, Oak Ridge, Tennessee, U.S.A. Accessed November 20, 2009.

2.2. FLUXNET data

We used in-situ measurements of ET from five FLUXNET forest sites. FLUXNET (http://fluxnet.ornl.gov/) is an international ecosystem network linking eddy covariance flux towers across different ecosystems. Original half-hourly measurements were preprocessed to ensure consistency among sites and reduce uncertainties in the computed fluxes (Restrepo-Coupe et al., 2013); this included general quality control assessment, and removal of outliers. Furthermore, in order to avoid the influence of water on the canopy, we used only daily data without precipitation during the previous 24 h. We aggregated fluxes and other meteorological data to daily values where at least 21–24 h of observations were available and then aggregated to 8-day time periods if at least 2–8 days were available. From a more complete database of fluxes and meteorological variables, we sampled: latent energy flux (LE, W/m^2), air temperature (Ta, °C), mean daily precipitation (Prec, mm), relative humidity (RH, %), short wave incoming radiation (SW, W/m^2), long wave incoming radiation (LW, W/m^2), sensible heat (H, W/m^2), net radiation (Rn, W/m^2). We determined top of the atmosphere radiation (TOA, W/m^2) following Goudriaan (1986).

We focused our investigation on forest areas located in USA and Australia, characterized by different vegetation types including deciduous broadleaf forest (DBF), evergreen needle leaf forest (ENF) and broadleaf deciduous forest (EDF). We selected sites with more than four years of data and overlapping with AMSR-E 2002–2006 coverage, and sites with homogenous land cover (defined as pixels with more than 50% of the area belonging to the same landcover in both the 1 km MODIS pixels and AMSR-E 25 km pixels). The homogeneous pixels were identified using the 1 km resolution MODIS (MOD12Q1) IGBP global land cover classification (Knowles, 2004). The only exceptions are the Tumbarumba and Willow Creek sites, in which the homogeneity of the land cover at 25 km is around 50%.

2.3. Land surface evapotranspiration retrieval

Remote sensing and flux tower observations were used to evaluate linear regression models, and the Penman–Monteith (PM)-Gs approach to estimate ET (Fig. 1). The direct regression approach combined flux tower measurements of ET with time-series of satellite indices. The PM-Gs uses an empirical relationship between Gs and different satellite indices to parameterize the conductance term of the PM equation (Eq. (1)) (Monteith, 1964). The remotely sensed-derived Gs (see Section 2.4) with other meteorological drivers were used as inputs into the PM equation to estimate ET.

$$\mathrm{LE} = \lfloor \frac{\epsilon \times A + (C_p \times \rho a/\gamma)[e_s(\mathrm{Ta}) - e_a] \times \mathrm{Ga}}{\epsilon + 1 + (\frac{\mathrm{Ga}}{\mathrm{Gs}})} \rfloor \quad (1)$$

where e_a is the vapor pressure in the air (kPa), e_s is the saturation vapor pressure evaluated at the air temperature (kPa), $\epsilon = s/\gamma$, in which s is the slope of the saturation vapor pressure versus temperature curve (kPa/°C) and γ is the psychrometric constant (kPa/°C), LE is latent energy (W/m^2), ρ_a is the mean air density at constant pressure (kg/m^3), C_p is the specific heat of the air (J/kg K), A (W/m^2) is the available energy absorbed by the surface (net absorbed radiation minus soil heat flux), G_s (m/s) and G_a (m/s) are the surface and aerodynamic (Eqs. (2) and (3)) conductance. ET (mm/day) is calculated as the ratio of LE: lambda, where lambda is the latent heat of vaporization (MJ/kg).

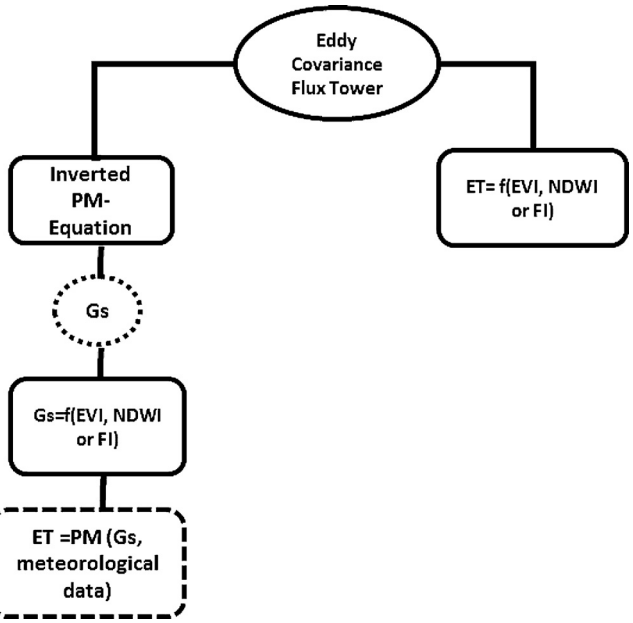

Fig. 1. Methodological flowchart. ET: evapotranspiration, PM: Penman–Monteith, Gs: Surface conductance, VIs: Vegetation index, FI: Frequency index.

$$\mathrm{ra} = \frac{1}{k^2 \mu} \ln(\frac{z-d}{z_o}) \ln(\frac{z-d}{z_{oH}}) \quad (2)$$

$$\mathrm{Ga} = \frac{1}{r_a} \quad (3)$$

where r_a is the aerodynamic resistance (s/m), μ the wind velocity (m/s) measured height (z), d the zero-plane displacement at z_o and z_{oH} the roughness lengths for momentum and heat respectively (m). The quantities d, z_o and z_{oH} were estimated as $d = 2\,h/3$ (m), 0.123 h and 0.0123 h respectively, where h is canopy height (see Table 1).

Eq. (1) implies that the energy balance is closed, i.e. the available energy equals the sum of latent and sensible heat exchange. This assumption is frequently not fulfilled by the eddy covariance (EC) method (Leuning et al., 2012; Wilson et al., 2002), although it is thought to be the most direct micrometeorological technique for measuring surface fluxes (Meyers and Baldocchi, 2005). Given the nature of the energy storage terms, a better energy closure can be achieved on a daily or seasonal basis (over which timescales the storage terms approach zero); however, as our 8-days Gs estimates are based on hourly values, we removed those times that may reflect an anomalous meteorological condition (e.g., advection) and will make the PM equation unstable. We used the energy balance closure to select these times and removed values where measurements of the turbulent energy exceeded linear regression estimates by 3 standard deviations or more.

To perform an evaluation of the relation between microwave/optical indices and LE observations, the coefficient of regression (r^2) using a linear regression type II between LE estimation and observation; the root mean square error (RMSE); the systematic root mean square error (RMSE$_s$); and unsystematic root mean square error (RMSE$_u$) were chosen as evaluation met-

Table 1
Spectral indices calculated from MODIS and AMSR-E, including their acronym, mathematical formulation and references. Where is the reflectance in MODIS band X (1: red, 2: near infrared, and 3: blue); l is the canopy background adjustment for correcting nonlinear, differential NIR and red radiant transfer through a canopy; c1 and c2 are the coefficients of the aerosol resistance term (which uses the blue band to correct for aerosol influences in the red band). In the frequency index formulation, Tb is the brightness temperature, and v suffixes indicate vertical polarization.

Index	Formulation	Reference
Frequency index	$FI = \frac{Tbv(Kaband) - Tbv(Xband)}{Tbv(Kaband) + Tbv(Xband)} \times 2$	Ferrazzoli et al. (1995)
Enhanced vegetation index	$EVI = \frac{2.5 \times (\rho 2 - \rho 1)}{(\rho 2 + 6 \times \rho 1 - 7.5 \times \rho 3 + 1)}$	Huete et al. (2002)
Normalized difference water index	$NDWI = \frac{\rho 2 - \rho 5}{\rho 2 + \rho 5}$	Hardisky (1983)

Table 2
Description of eddy covariance flux tower sites used in this study. Where *h* is canopy height, *Z* is measurement height, DBF is deciduous broadleaf forest, and ENF and EBF: are evergreen needleaf and broadleaf forest respectively. IGBP is the International Geosphere–Biosphere Programme vegetation classification.

Code	Name	Country	Lat	Lon	*h*(m)	*Z*(m)	IGBP	Years	References
US-Ha1	MA – Harvard Forest EMS Tower (HFR1)	United States	42.54	−72.17	22	31	DBF	2000–2006	Urbanski et al. (2007)
US-MMS	IN – Morgan Monroe State Forest	United States	39.32	−86.41	25	48	DBF	2000–2005	Schmid et al. (2000)
US-WCr	WI – Willow Creek	United States	45.81	−90.08	24	30	DBF	2000–2006	Cook (2008)
US-Ho1	ME – Howland Forest (main tower)	United States	45.2	−68.74	20	29	ENF	2000–2004	Hollinger et al. (2004)
AU-Tum	Tumbarumba	Australia	−35.66	147.15	40	70	EBF	2001–2006	Leuning et al. (2005)

rics. A good model was considered to have a high r^2 value, a low total RMSE and RMSEs ≈ 0. Our results were compared to other published studies in the discussion. These studies provided RMSE estimates against mean flux tower LE estimates in W/m^2.

2.4. Surface conductance retrieval

The surface conductance (Gs) plays an active role in limiting ET and is in itself a function of vegetation and environmental variables, including Ta, VPD, water potential, photosynthetic active radiation (PAR), and ambient carbon dioxide concentration (CO_2) (Monteith, 1985; Monteith, 1985). In this framework, two different approaches were tested to estimate surface conductance (Gs) over the growing season using FI and vegetation optical indices (VIs): single-sensor vs. multi-sensor (Table 1 and Fig. 2). Using meteorological and flux tower data we calculated Gs under the PM-equation (Eq. (4)) needed for the calibration and validation analysis with satellite indices.

$$G_s = \left\lfloor \frac{LE \times Ga}{\epsilon \times A - (\epsilon + 1) \times LE + \left(\frac{C_p \cdot \times \rho_{aGa}[e_s(Ta) - e_a]}{\gamma}\right)} \right\rfloor \quad (4)$$

For the individual approaches, we used an exponential equation to estimate Gs from VIs as in Yebra et al. (2013) (equation: $Gs = a \times e\hat{}(b \times VIs) + c$, where c is the intercept, a and b are the partial regression coefficients). and a polynomial regression (equation: $Gs = a \times FI + b \times FI\hat{}2 + c$, where c is the intercept, a and b are the partial regression coefficients) to estimate Gs from the microwave index (Li et al., 2009).

Two multivariable models were developed using the optical and passive microwave indices at 25 km to estimate Gs. The aim of these approaches was to improve Gs estimations based on multiple observations that combine two important variables (vegetation moisture and leaf photosynthesis). One methodology was based on a stepwise multiple linear regression that fits an observed dependent data set (Gs) using a linear combination of independent variables (equation: $Gs = a \times Gs\ (VIs) + b \times Gs\ (FI) + c$, where c is the intercept, a and b are the partial regression coefficients, Gs (VIs) is the surface conducted estimated using optical indices and Gs (FI) is the surface conducted estimated using passive microwave index).

The second multivariable model was based on a strategy for combining Gs_{VI} and Gs_{FI} indices as follows (Fig. 2): we used the best upscale Gs_{VI}, Gs_{FI} or Gs_{VI-FI} model as a default value dependent upon; if Gs_{VI} or $Gs_{VI\text{-}FI}$ was the default value and a VI observation was missing at a time when an AMSR-E observation exist, we replaced the missing Gs_{VI} or Gs_{VI-FI} data with Gs_{FI}.

To evaluate the relation between satellite indices and Gs observations, we calculated the coefficient of regression (r^2) using a linear regression type II from a pool of data to calibrate the equation between satellite indices and Gs observations. The pooled dataset contained 185 8-days observations (randomly selected) that were used to calibrate the relationships between the vegetation indices (optical and passive microwave indices) and Gs. The rest, 618 8-days observations, were used to validate these approaches. Adjusted coefficient of regression (r^2_{adj}) was calculated for the stepwise multiple linear regression. We also calculated the r^2 and the root mean square error (RMSE) between Gs estimation and observation, with the calibration dataset and with the rest of the sample (validation dataset). A good model was considered to have a high r^2 value, and a low total RMSE (RMSE ≈ 0).

3. Results

3.1. Calibration of surface conductance (Gs) models

3.1.1. Relation between optical indices and Gs at 1 km

The relation between Gs and vegetation optical indices are shown in Table 3 (see Supplementary material Fig. S01). As reported in Yebra et al. (2013), there was a nonlinear relation between Gs and both optical indices (EVI and NDWI). The regression results showed non-significant relations between the VIs and Gs at Tumbarumba, due to the lack of EVI and NDWI seasonality in the calibration and validation dataset (Table 3). At Howland Forest and Harvard Forest, the VIs also showed a low and non-significant regression with Gs. The others sites presented a better fit, $r^2 > 0.4$ for all VIs for calibration and validation dataset.

The EVI and NDWI models presented the similar coefficient of determination (higher than 0.5) and the RMSE was lower than 4.0 mm/s across two of the deciduous forest areas (Morgan Monroe State Forest (MMS) and Willow Creek (WCr)) for calibration and validation (Table 3). For the other deciduous forest site, Harvard Forest (Ha1), and for the mixed evergreen needleleaf and broadleaf forests of Howland Forest (Ho1), the NDWI and EVI model explained only 20% of the Gs variation. These results showed that both VIs could explain the variation of Gs over deciduous forests.

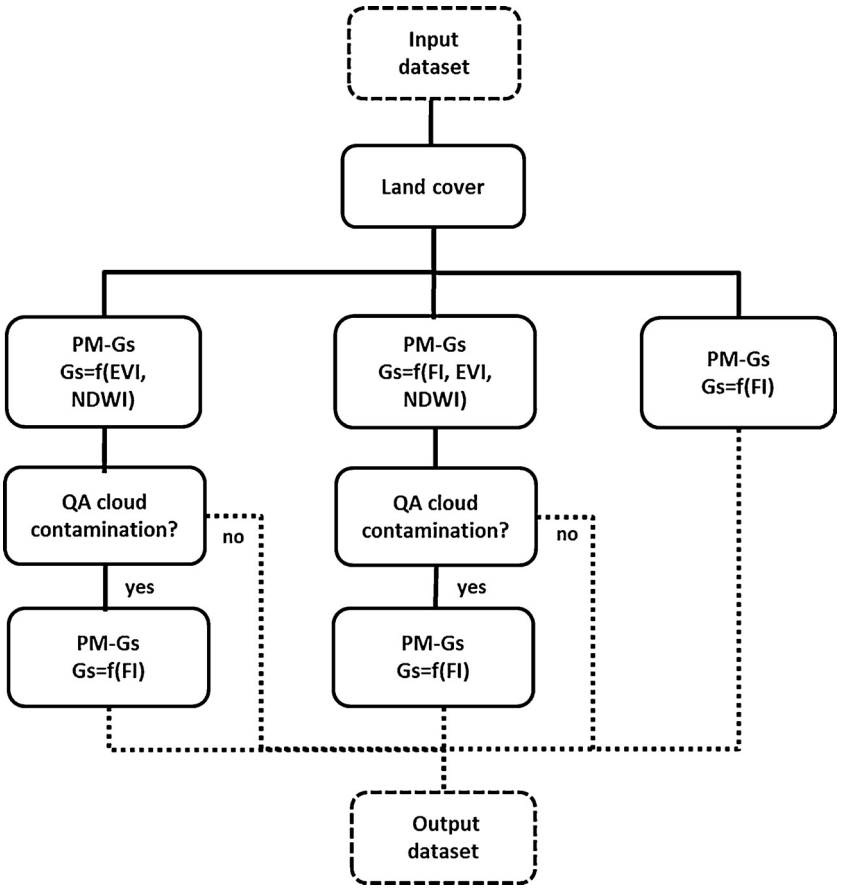

Fig. 2. Methodology flowchart for the Surface conductance (Gs) output dataset resulting from combining optical and passive microwave indices. PM: Penman–Monteith, EVI: enhanced vegetation index, NDWI: Normalized difference water index, FI: Frequency index. Input dataset: MODIS VIs and AMSR-E FI indices, QA: quality assessment.

Table 3
Summary of the relation between optical indices and surface conductance (Gs). Where $r^2_{VI\text{-}Gs}$ is coefficient of determination between satellite indices and Gs observations, $r^2_{Gso\text{-}Gse}$ is coefficient of determination and RMSE root mean square error between Gs observation and estimations. A logarithmic transformation has been made over the nonlinear relation between optical indices and Gs.

Name	IGBP	Calibration						Validation			
		EVI			NDWI			EVI		NDWI	
		$r^2_{VI\text{-}Gs}$	$r^2_{Gso\text{-}Gse}$	RMSE (mm/s)	$r^2_{VI\text{-}Gs}$	$r^2_{Gso\text{-}Gse}$	RMSE (mm/s)	$r^2_{Gso\text{-}Gse}$	RMSE (mm/s)	$r^2_{Gso\text{-}Gse}$	RMSE (mm/s)
Tum	EBF	0.00	0.02	4.72	0.00	0.01	4.73	0.01	4.10	0.00	3.03
Ho1	ENF	0.22	0.19	2.35	0.24	0.19	2.33	0.10	2.74	0.07	3.43
Ha1	DBF	0.14	0.23	3.03	0.22	0.22	3.05	0.21	2.76	0.30	2.62
MMS	DBF	0.80	0.50	3.22	0.80	0.46	3.34	0.44	3.32	0.39	3.54
WCr	DBF	0.73	0.75	2.52	0.71	0.67	2.93	0.63	3.29	0.50	3.94

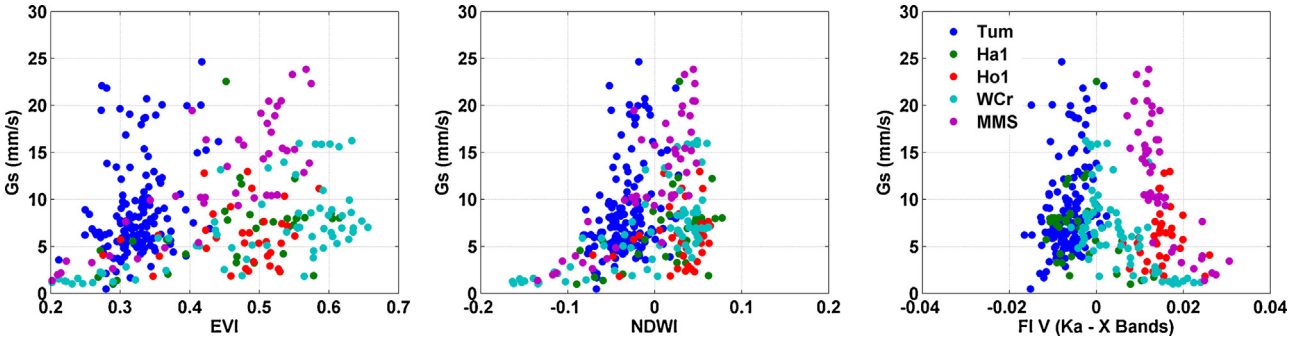

Fig. 3. Relation between Gs (surface conductance, mm/s) and vegetation indices.

Table 4
Parameter estimates as well as coefficient of determination (r^2) for the models using the calibration dataset. Where a–c are the parameters of each equations, $r^2_{VI\text{-}Gs}$ is coefficient of determination between optical indices and Gs observations, $r^2_{FI\text{-}Gs}$ is coefficient of determination between passive microwave indices and Gs observations, and r^2_{adj} is the adjusted coefficient of determination. A logarithmic transformation was made over the nonlinear relations between optical indices and Gs.

Name	IGBP	EVI Gs= $a \times e\hat{}(b \times \text{EVI}) + c$				NDWI Gs = $a \times e\hat{}(b \times \text{NDWI}) + c$				FI Gs = $a \times \text{FI} + b \times \text{FI}\hat{2} + c$			
		a	b	c	$r^2_{VI\text{-}Gs}$	a	b	c	$r^2_{VI\text{-}Gs}$	a	b	c	$r^2_{FI\text{-}Gs}$
Tum	EBF	7.07	0.13	7.76	0.05	-3.72e5	3.71e5	3.12e-5	0.12	616.03	0.18e4	11.63	0.28
Ho1	ENF	6.45	−1.16e4	−27.31	0.33	−1.43e5	1.43e5	1.25e-4	0.14	1.14e3	−3.42e4	−2.77	0.20
Ha1	DBF	5.41	0.05	6.46	0.71	−2.88e5	2.88e5	2.15e-4	0.30	−231.44	−2.16e4	6.91	0.79
MMS	DBF	63.22	−65.61	−0.27	0.64	−8.58e5	8.58e5	3.12e-5	0.40	−250.79	−5.51e3	−2.78	0.69
WCr	DBF	46.63	−54.28	−0.94	0.69	−9.85	22.87	3.29	0.41	−1.45e3	1.52e4	30.68	0.64

Name	IGBP	EVI, FI Gs = $a \times$ Gs (EVI) + $b \times$ Gs (FI) + c					NDWI, FI Gs = $a \times$ Gs (NDWI) + $b \times$ Gs (FI) + c				
		a	b	c	$r^2_{FI,\,VI\text{-}Gs}$	r^2_{adj}	a	b	c	$r^2_{FI,\,VI\text{-}Gs}$	r^2_{adj}
Tum	EBF	1.1	1.76	−11.29	0.2	0.18	0.82	0.73	−4.88	0.11	0.1
Ho1	ENF	0.83	1	8.02E-08	0.19	0.17	0.3	1	8.02E-08	0.2	0.17
Ha1	DBF	0.47	1	1.25E-07	0.22	0.21	1	0.47	−5.52E-10	0.27	0.25
MMS	DBF	1	0.24	−8.03E-08	0.44	0.43	1	0.19	0	0.46	0.45
WCr	DBF	1	0.22	1.41E-10	0.67	0.67	1	0.25	0	0.68	0.67

3.1.2. Relations between microwave and optical indices with Gs at 25 km

Fig. 3 shows the relation between Gs and optical (using the aggregated VIs at 25 km) and passive microwave indices. Table 4 shows the parameters estimates as well as coefficients of determination (r^2) derived from the linear regression between VIs and FI indices using the calibration dataset. The EVI models derived from the PM-Gs approach had consistently a better fit than NDWI, with $r^2 > 0.60$ for all deciduous forests. The NDWI model showed a better fit than EVI for Tum explaining only 10% of the Gs variance; however the FI model explained more than 20%. We also found that the combined EVI-FI model performed well for Tum, and the NDWI-FI model performed better for Ho1. For the other sites, the multiple regression analysis did not provide more information than the individual models.

Using the parameters mentioned in Table 4 we evaluated the accuracy of all models over the calibration and validation datasets based upon their RMSE and r^2 between estimated and observed Gs (Table 5). For the individual optical indices, the EVI model explained between 30 and 60% of the variance of Gs for DBF, with a RSME between 2.5–3.0 mm/s for validation and calibration dataset. For deciduous forests, FI model showed similar r^2 with high RSME compare to the optical indices. However, the optical indices had better regression coefficients and less RMSE than the microwave model (Table 5). The NDWI models showed the best performance for evergreen forests, but only explained less than 10% of the variance of Gs for both datasets. For the evergreen needleleaf forests, the FI model presented better performance compared to the optical indices.

The multiple regression models improved the estimations of Gs for the evergreen forest. For Ha1, in spite of the higher determination coefficient of the multiple regression models the RMSE was higher than individual approach. All these results shows that there was not a unique index that performed best for all the deciduous and the evergreen forest. This made the PM-Gs methodology a land cover depended algorithm.

Interestingly, the multivariable model using EVI and FI improved the estimation of Gs for Tum, explaining 20% of the variance in Gs (for calibration and validation analysis) with the lowest RMSE. At Tumbarumba site, the Eucalyptus forest is moderately open and has an average tree height of roughly 40 m. The canopy is roughly divided into two layers. There is also significant ground cover of shrubs and grasses (Jupp et al., 2009; Strahler et al., 2008). To evaluate if this improvement was related to the presence of other layers (shrubs and grasses), we estimated Gs using NDWI at different win-

Table 5
Summary of the comparison between Gs estimation and observation using Gs (VIs) model, Gs (FI) model, and multivariable model (Gs (VIs, FI)). Where the coefficient of determination ($r^2_{Gso\text{-}Gse}$) and root mean square error (RMSE) were calculated between Gs estimations and observations.

Calibration

Name	IGBP	Gs (EVI)		Gs (NDWI)		Gs (FI)		Gs (EVI, FI)		Gs (NDWI, FI)	
		$r^2_{Gso\text{-}Gse}$	RMSE (mm/s)	$r^2_{Gso\text{-}Gse}$	RMSE (mm/s)	$r^2_{Gso\text{-}Gse}$	RMSE (mm/s)	$r^2_{Gso\text{-}Gse}$	RMSE (mm/s)	$r^2_{Gso\text{-}Gse}$	RMSE (mm/s)
Tum	EBF	0.01	4.07	0.02	1.05	0.03	4.88	0.20	4.61	0.11	4.85
Ho1	ENF	0.10	2.65	0.12	2.63	0.17	2.62	0.25	2.77	0.20	2.77
Ha1	DBF	0.35	2.49	0.31	2.57	0.23	3.44	0.25	3.55	0.30	3.46
MMS	DBF	0.45	3.06	0.38	3.25	0.38	3.30	0.44	3.28	0.50	3.19
WCr	DBF	0.66	3.19	0.55	3.69	0.59	4.65	0.68	4.07	0.69	4.03

Validation

Name	IGBP	Gs (EVI)		Gs (NDWI)		Gs (FI)		Gs (EVI, FI)		Gs (NDWI, FI)	
		$r^2_{Gso\text{-}Gse}$	RMSE (mm/s)	$r^2_{Gso\text{-}Gse}$	RMSE (mm/s)	$r^2_{Gso\text{-}Gse}$	RMSE (mm/s)	$r^2_{Gso\text{-}Gse}$	RMSE (mm/s)	$r^2_{Gso\text{-}Gse}$	RMSE (mm/s)
Tum	EBF	0.07	4.04	0.10	4.08	0.10	3.89	0.20	3.77	0.12	3.89
Ho1	ENF	0.02	3.61	0.10	3.02	0.20	2.65	0.14	5.75	0.23	3.38
Ha1	DBF	0.27	2.79	0.40	2.93	0.36	2.49	0.41	4.36	0.50	5.01
MMS	DBF	0.44	3.39	0.46	3.32	0.43	3.17	0.47	3.17	0.49	3.40
WCr	DBF	0.63	3.46	0.59	4.31	0.57	4.12	0.65	3.73	0.58	5.62

Table 6
Summary of the relation between predicted versus measured 8-day latent heat (LE (W/m^2)) directly derived from optical and passive microwave indices. Where r^2_{VI-LE} is the coefficient of determination between optical indices and LE measures, r^2_{FI-LE} is the coefficient of determination between passive microwave indices and LE measures, and RMSE the root mean square error, RMSEs the systematic root mean square error and RMSEu unsystematic root mean square error for the best models.

Name	IGBP	VI				FI			
		r^2_{VI-LE}	RMSE (W/m^2)	RMSEu (W/m^2)	RMSEs (W/m^2)	r^2_{FI-LE}	RMSE (W/m^2)	RMSEu (W/m^2)	RMSEs (W/m^2)
Tum	EBF	0.36(NDWI)	24.66	14.85	19.68	0.04	31.27	2.52	31.17
Ho1	ENF	0.51 (EVI)	17.57	12.56	12.29	0,30	22.07	11.22	19.01
Ha1	DBF	0.56 (EVI)	20.51	15.41	13.52	0.30	26.25	14.30	22.01
MMS	DBF	0.72 (EVI)	20.73	17.60	10.92	0.75	20.32	17.78	10.22
WCr	DBF	0.62 (EVI)	19.33	15.26	11.87	0.47	22.56	15.52	16.35

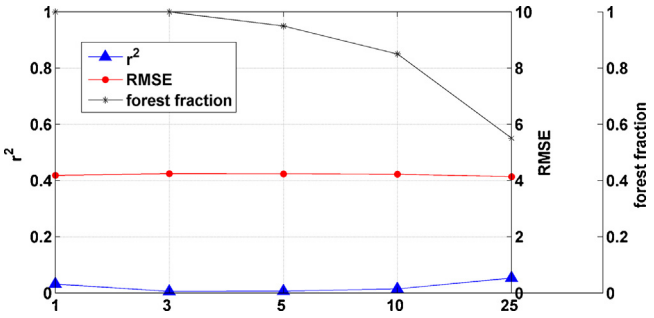

Fig. 4. Relation between surface conductance estimations using the NDWI and surface conductance (Gs) observation at different windows size (from 1 to 25 km). r^2 is the coefficient of determination and RMSE root mean square error between Gs observation and estimations, and the fraction of forest inside the pixel size. The fraction of forest was calculated using the MODIS (MOD12Q1) IGBP global land cover classification product (Knowles, 2004).

dow sizes (Fig. 4). In spite of the decrease of the forest cover, the optical approach did not improve.

For our final analysis we used PM-Gs methodology, combining optical and passive microwave data to obtain a complete time series (multivariable model II, Fig. 2). For evergreen forests, the FI- model and the multivariable model showed higher r^2 and lower RMSE compared to the optical model. Interestingly, for deciduous forests the optical model showed the best approach, but with the lowest number of samples.

3.2. Evapotranspiration model performance evaluation

We compared and evaluated two methodologies to estimate ET: (1) direct regression and (2) PM-Gs approach. In the direction regression method, EVI had a good performance at almost all forest sites; with the exception of Tumbarumba, where NDWI had a higher accuracy (Table 6). At Tumbarumba, the VIs and FI did not exhibit a clear seasonality (low amplitude annual cycle), thus reducing the correlation between ET and VI compared to the other forests. The r^2 values were lower than 0.7 and the RMSE greater than 20 W/m^2 for all VIs and FI. In general, the RMSEs was greater than RMSEu. Fig. 5 shows the relation between vegetation indices and LE, and the relation between observed and estimated LE. In summary, VI–LE relations showed a lower RMSE and higher r^2 than the FI–LE approach. However, both direct approaches underestimates at large LE values as shown in Fig. 6. Furthermore, there was a tendency to overestimate at lower values of LE.

Overall, we observed a good agreement between estimated and observed LE for both optical and passive microwave indices using the PM-Gs approaches (Table 7). For the optical model we used EVI and NDWI as shown in Table 5. In general, PM-Gs (VI) and PM-Gs (FI) approach explained more than 70% of the variance of ET. However, PM-Gs (FI) had higher RMSE values than the optical data. In general, systematic differences (RMSEs) between model predictions and observations were lower than the non-systematic error (RMSEu). Since RMSE was mostly composed of RMSEu, the model RMSE was probably as low as possible, and their values were similar with those reported previously (Li et al., 2009; Yebra et al., 2013).

Fig. 8 shows the relation between observed and estimated LE as a function of Gs relative error (%) for all the sites together and Gs estimations versus Gs observations, showing the overall uncertainties (r^2 and RMSE) for LE and Gs. The ensemble of PM-Gs (VIs) accounted for 69% of the variance of LE (RSME = 22.60 W/m^2). PM-Gs (FI) accounted for 70% of the variance of LE with RSME = 22.65 W/m^2. Combining optical and passive microwave vegetation models (multivariable model II) resulted in the best performance (high r^2, lower RMSE and high n) (Fig. 8). Furthermore, the coupled model II incorporated a higher number for samples compared to the individual PM-Gs approach without sacrificing the precision.

Fig. 8 shows LE estimations versus LE observations for evergreen and deciduous forests. For evergreen forests, we obtain a higher r^2 and lower RMSE compared to the individually derived (VI or FI)

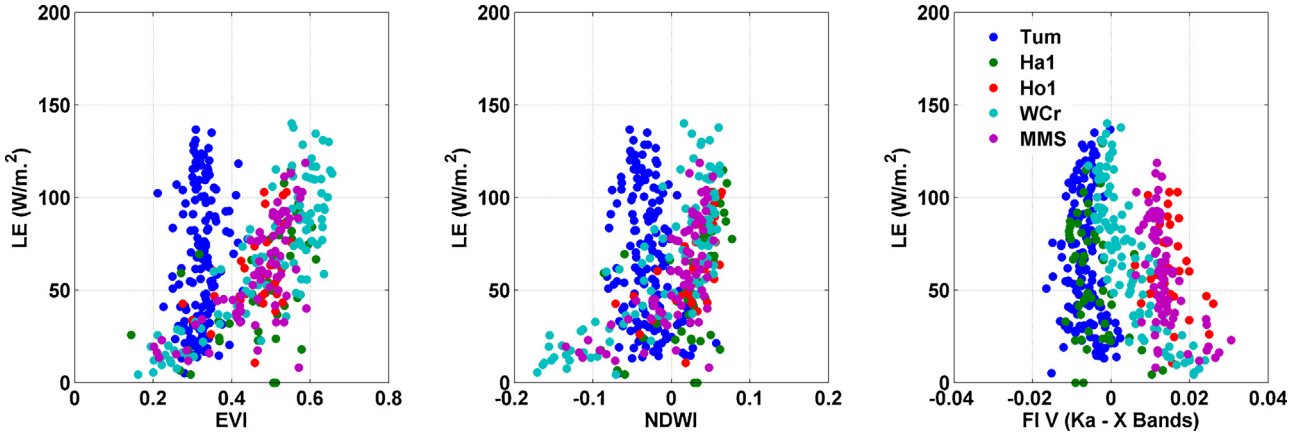

Fig. 5. Relationship between Gs (surface conductance, mm/s) and vegetation indices.

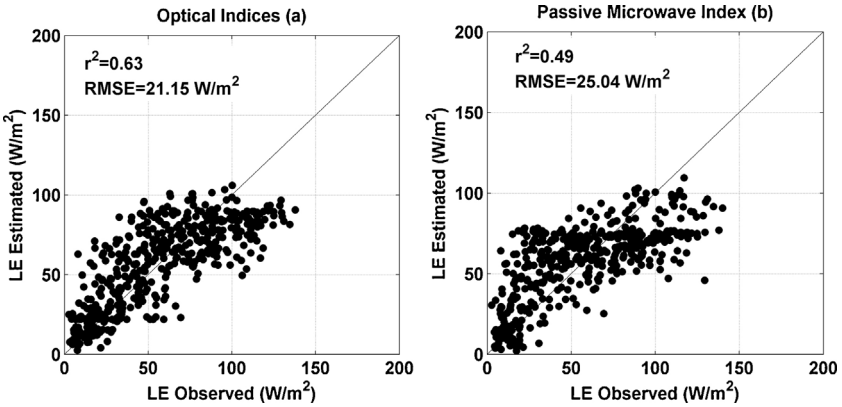

Fig. 6. Predicted versus measured 8-day latent heat (LE (W/m^2))directly derived from (a) optical indices (see Table 7 for VIs) and (b) FI.

Table 7
Summary of the relation between predicted versus measured 8-day latent heat (LE (W/m^2)) within the PM framework. Where $r^2_{LEo\text{-}LEe}$ is the coefficient of determination between LE measures and LE estimations, RMSE the root mean square error, RMSEs the systematic root mean square error and RMSEu unsystematic root mean square error for the best models. n is the number of 8-day periods with valid tower, MODIS and AMSR-E derived measurements.

Name	IGBP	VI				
		n	$r^2_{LEo\text{-}LEe}$	RMSE (W/m^2)	RMSEu (W/m^2)	RMSEs (W/m^2)
Tum	EBF	136	0.71	26.67	19.39	18.32
Ho1	ENF	37	0.27	25.82	20.40	15.85
Ha1	DBF	40	0.61	18.80	17.56	6.73
MMS	DBF	70	0.75	19.93	19.77	2.55
WCr	DBF	47	0.87	9.45	9.36	1.28
		FI				
Tum	EBF	175	0.69	26.59	25.42	7.78
Ho1	ENF	62	0.37	20.59	17.68	10.55
Ha1	DBF	53	0.72	16.71	13.63	9.66
MMS	DBF	86	0.73	21.81	20.83	6.47
WCr	DBF	40	0.74	14.98	13.91	5.56
		VI–FI				
Tum	EBF	230	0.72	24.55	23.81	6.00
Ho1	ENF	62	0.37	20.58	17.68	10.55
Ha1	DBF	108	0.72	17.71	13.44	11.54
MMS	DBF	118	0.71	21.68	18.56	11.20
WCr	DBF	100	0.70	17.36	14.26	9.89

LE. Interestingly, the multivariable model II resulted in the best performance for evergreen forests (Fig. 8a–c). However, the variability in modeled LE estimates from Fig. 8 showed scatter along the 1:1 line, with a tendency to overestimate at higher LE ranges. For deciduous forests, the individual methodology presented a better performance (Fig. 8d and e); however the numbers of samples increased to 50% using the multivariable-model II (Fig. 8f).

Fig. 9 shows direct comparison between observed and estimated LE as a function of time for both growing seasons between 2002 and 2006. The predicted LE using these three approaches captures the seasonal variation very well in the transient periods and during stable state of the growing season. It implies that these models could represent the seasonality of vegetation state. However, for Tumbarumba there was an overestimation during the stable state of the growing season.

4. Discussion

This study applied the Penman–Monteith (PM) model and direct regressions to estimate ET from forest ecosystems at 8-day time scales using optical and passive microwave indices. In our analysis, we considered 5 forest sites, representing three forest types: DBF, EBF and ENF. The PM-Gs approach provided ET estimates that were better than estimates derived from direct regressions between VIs and FI and measured LE. An underestimation effect was observed in both LE–VIs and LE–FI relationship for large LE values across the forest cover types, as shown by the higher values of RMSE compared to RMSEu. However, we found consistencies between independent satellite (optical and passive microwave indices) and in situ tower G_S relationships, and then with LE. In general, the PM-models explained more than 70% of the variance in LE with RMSE lower than 20 W/m^2. RMSE values found in this study are commensurate with those reported previously (Kalma et al., 2008; Li et al., 2009; Yebra et al., 2013). The mean difference between estimated and observed LE was ~30%, which agreed with errors reported in the literature. It is relevant to mentioned that for these study areas LE was driven primarily by surface meteorology. For these reasons, the performance of the LE model was much better than for Gs model. However, overestimates of Gs in some biomes result in overestimates of LE even if other inputs such as the meteorological data are relatively accurate (Fig. 8). In this case, better estimations of Gs would improve the retrieval of LE.

Optical and passive microwave index approaches provided independent estimations of Gs at the same time (AMSR-E and MODIS sensors are both on the AQUA platform) based on different biophysical processes. Optical vegetation indices are mainly sen-

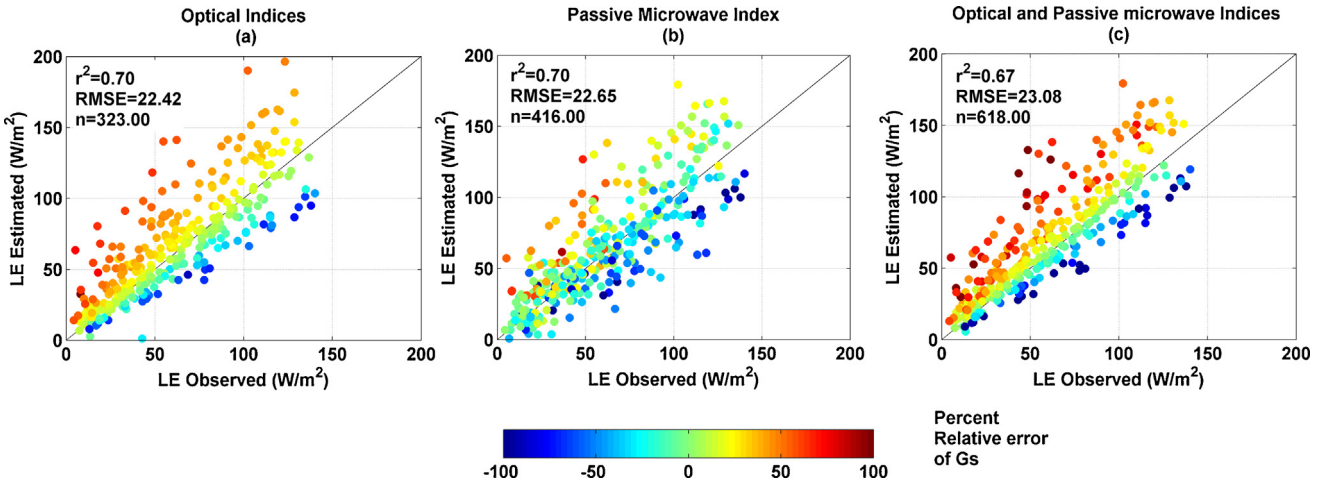

Fig. 7. Predicted versus measured 8-day and latent heat (LE (W/m^2)) derived from optical indices showing in Table 5 (a), FI (b) and both indices (c) combined with meteorological data within the PM framework. Colorbar represent % relative error of Gs. n is the number of 8-day periods with valid tower, MODIS and AMSR-E derived measurements.

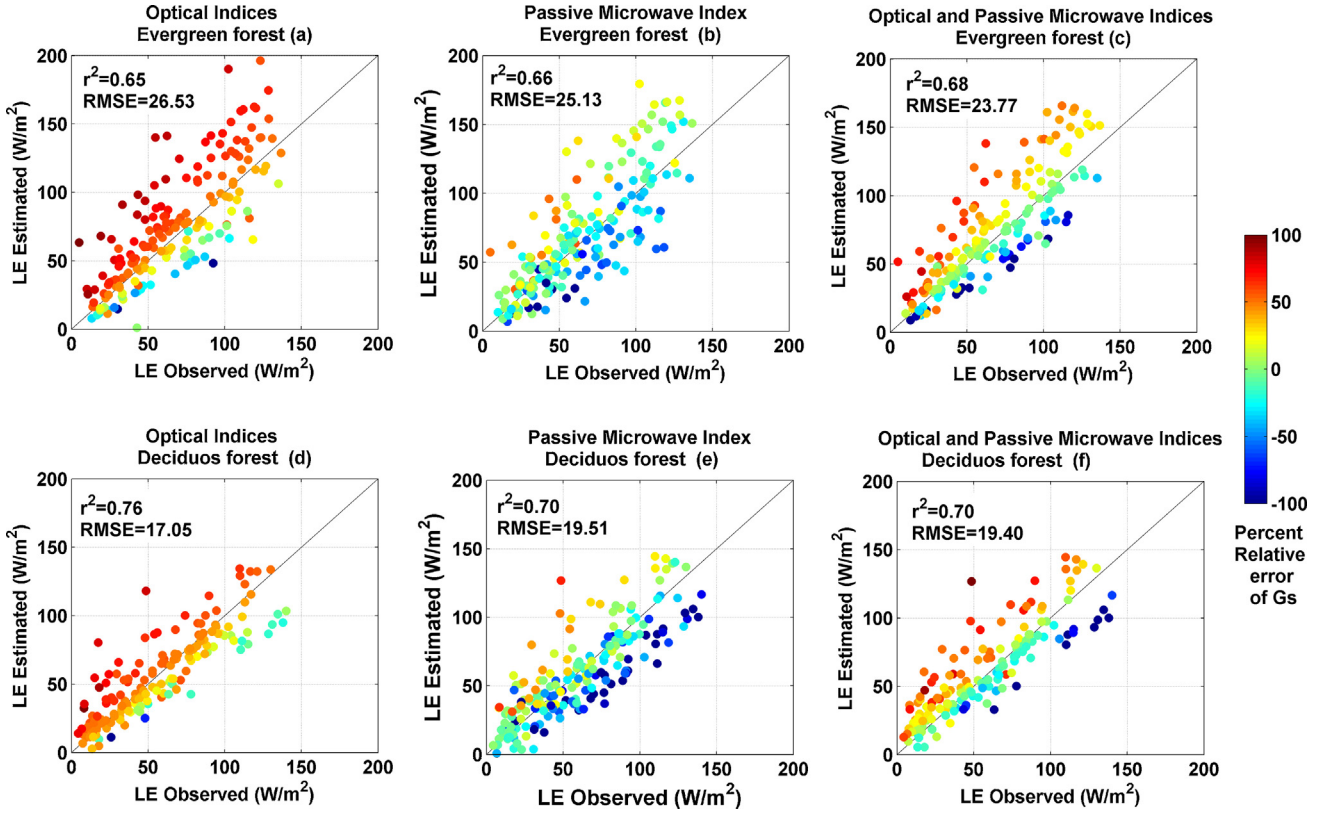

Fig. 8. Predicted versus measured 8-day latent heat (LE (W/m^2)) derived from optical indices showing in Table 4 (a and d), FI (b and e), and both indices (c and f) model combined with meteorological data within the PM framework for evergreen and deciduous forest. Colorbar represent % relative error of Gs. *n* is the number of 8-day periods with valid tower, MODIS and AMSR-E derived measurements.

sitive to seasonal changes of vegetation foliage while microwave indices provide unique information about the forest canopy water content, including greater penetration and sensitivity to both the leafy and woody components.

Satisfactory agreements were obtained between 8-day Gs and passive microwave and optical indices. We have shown that NDWI and EVI correlate well with Gs for deciduous forest, allowing the use of remote sensing observations to estimate this parameter under the PM framework. However, in contrast to Yebra et al. (2013) there was not a significant difference in the performance of EVI and NDWI. Since Gs is closely related to leaf chlorophyll concentration (Matsumoto et al., 2005) and the leaf turgor and structure (Bowman, 1989), a good correlation between Gs and EVI was expected. Good correlations were also expected between NDWI and Gs, which was reported to be sensitive to leaf water content (Guerschman et al., 2009).

We expected a better accuracy of Gs estimations using optical indices at 1 km due to the better spatial resolution. Optical VIs (at 25 km) showed similar r^2 to FI, however, lower RMSE. Scale inconsistencies have certain effects on the evaluation and com-

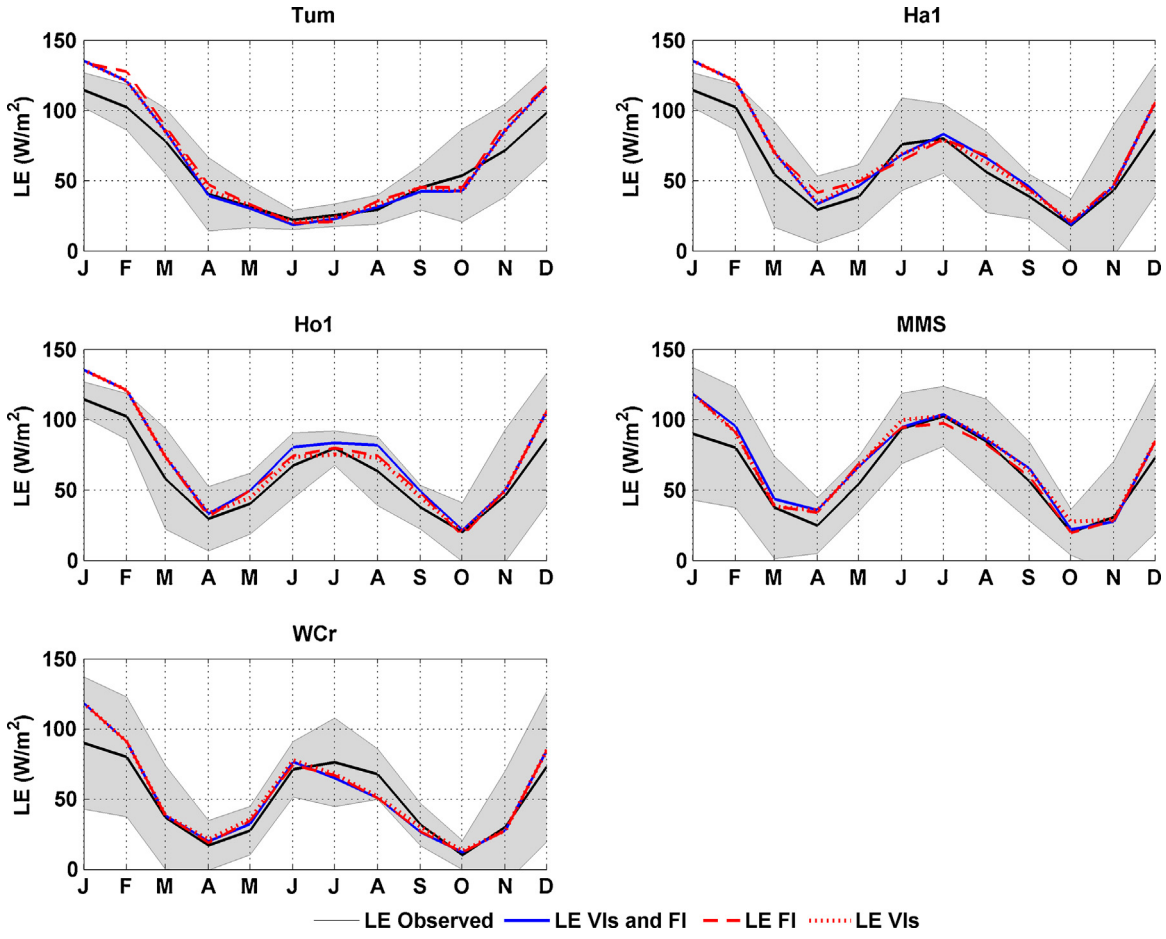

Fig. 9. Time series of predicted and measured 8-day latent heat (LE (W/m^2)) derived from optical indices shown in Table 4 (LE VIs), FI (LE FI), and both indices (LE VIs and FI) model combined with meteorological data within the PM framework.

parison of the satellite and surface data: (1) there are common errors associated with these measurements (Moncrieff et al., 1996; Richardson et al., 2006), though we dealt with these uncertainties by using a Type II regression, (2) eddy covariance fluxes and meteorological sensors (radiation, temperature, humidity have different footprints), and (3) the tower flux footprint is only a small fraction of the footprint of passive microwave systems (AMSR-E). To address the eddy covariance- remote sensing footprint issues, we evaluated optical indices with tower Gs estimations at different windows sizes (see Tables 3 and 5 and Supplementary material Fig. S02). Comparing these results, the RMSE was lower and the r^2 was higher at coarse spatial scales, indicating a spatial scaling effects. However, at AMSR-E spatial scales this methodology was able to capture subtle variations in Gs. The biophysical variables defining the homogeneity of optical indices for an area are not the same as those that define the homogeneity of passive microwave indices, which is a possible explanation of the observed discrepancies between optical and passive microwave model results for similar window size (Table 5).

Although some variances shown in this study may be explained by scale-inconsistence and observation uncertainties, more than 40% of variations in Gs are explained using microwave index time series, as it was also shown by Min and Lin, (2006). Microwave indices – EDVI in the case of Li et al. (2009) and FI for the current study (Barraza et al., 2014a) – are sensitive to vegetation moisture (water content in woody and leaf), which is an important component of the vegetation-atmosphere interaction. As FI is directly linked to vegetation moisture, the changes of FI represent canopy response to the changes of environmental conditions across different forest ecosystem. This is the key biophysical link that allows us to estimate Gs and ultimately accurately estimate LE based on a PM equation approach. Furthermore, over evergreen forest FI model performed better than optical indices. In this context, it is important to note that microwave radiation has much more penetration in vegetated areas than optical wavelengths, and overall canopy emission is an integration of microwave radiation from the whole canopy's vertical profile weighted by its transmission. This could be a reason of the improved performance of FI model over evergreen forest.

In this study we presented two different ways of using optical and passive microwave remote sensing: (1) stepwise multiple linear regressions and, (2) a combined Gs product of both VIs and FI (coupled model II). These multivariable models use an approach to estimate Gs at large scale that is based on different biophysical information from passive microwave and optical indices (vegetation moisture, leaf chlorophyll concentration, and leaf turgor and structure). At the evergreen forests, the multi-linear regression model showed the best performance compared to individual VIs models. For the other sites, this approach did not provide new information compared to independent models.

In spite of the better accuracy of VIs-Gs approach compared to FI-Gs for the other forest sites, Fig. 7 shows positive relative error, due to noise data. In some situations, quality flags (MODIS QA) are insufficient to reduce the noise in the MODIS products (Demarty et al., 2007). Smoothing filters can reduce the noise but this introduces artificial values (Mu et al., 2011). Passive microwave index is less affected than optical systems by atmospheric conditions, and in this study we showed a complementary approach to provide a

complete Gs time series. We developed a strategy for combining Gs_{VI} and Gs_{FI} estimations based on gap filling of low quality and noisy VI data. This last model (Figs. 7 and 8) that merged Gs product of both VIs and FI indices is feasible (in terms of higher r^2 and lower RMSE) and would decrease the amount of data gaps. These consistencies lend confidence to both datasets and offer opportunities for more extensive regional scaling of tower fluxes with satellite data. Consequently, the best LE and Gs performance was obtained by combining both time series (Figs. 7 and 8). In comparison to the Global canopy conductance (Gc) product, based on Yebra et al. (2013) methodology, using MODIS reflectance from MCD43C4 product and three vegetation indices (NDVI, EVI and crop factor (Kc)) at 0.05° and every 8 days, (https://data.csiro.au/dap/landingpage?pid=csiro%3A5946), our results presents a better accuracy (see Supplementary material Fig. S03 and Table S01). Since Gc is derived from PM equation, we could relate Gs observation with Gc product (Yebra et al., 2013). In spite of the scales problems between flux tower and passive microwave index (25 km), the results presented in this article shows an improved approach of Gs estimations for these forests.

Finally, it is important to mention that these results could be relevant in the context of land surface modeling, since time series of remotely-sensed Gs can be integrated with land surface models that use the PM approach. Furthermore, both estimations could present different applications depending on the scale resolution (e.g. ecological vs. climate applications). Further work is needed in order to evaluate how best to integrate spatially extensive satellite data with local tower measures from multiple sites for regional scaling and modeling of ET.

5. Conclusions

When MODIS VIs and passive microwave index were combined, the disadvantages of both sensors can be reduced in the context of ET estimations. Indices were combined to make use of the advantages of both sensors. This study shows that the estimation of Gs using either satellite optical or microwave indices has a number of advantages and disadvantages. The most important disadvantage of passive microwave is the lower spatial resolution. Optical data presents some limitations related to the low temporal resolution due to cloud and aerosol contamination. But optical indices have the advantages of: (i) high spatial resolution, (ii) sensitivity to the leafy part of the vegetation, while microwave indices advantages are: (i) higher temporal resolution at daily and hourly scales, (ii) day and nighttime measurements (Barraza et al., 2014a,b; Li et al., 2009), and (iii) sensitivity to the leafy and woody parts of the vegetation. Using a combined index-model integration approach leads to superior ET estimates.

Acknowledgments

Part of this study was conducted through a visiting scholar appointment awarded to the author by the University of Technology, Sydney through funds from ARC-DP140102698 (Huete, CI). This work was also funded by MinCyT-CONAE-CONICET project 12. The author thanks Fluxnet and Ozflux Network for making the data freely available as well as the flux tower principal investigators.

Appendix A. Supplementary data

Supplementary data associated with this article can be found, in the online version, at http://dx.doi.org/10.1016/j.agrformet.2015.06.020

References

Allen, R.G., Pereira, L.S., Raes, D., Smith, M., et al., 1998. Crop Evapotranspiration-guidelines for Computing Crop Water Requirements-FAO Irrigation and Drainage Paper 56. FAO, Rome, 300, 6541.

Andela, N., Liu, Y.Y., van Dijk, A.I.J.M., de Jeu, R.A.M., McVicar, T.R., 2008. Global changes in dryland vegetation dynamics (1988–2008) assessed by satellite remote sensing: comparing a new passive microwave vegetation density record with reflective greenness data. Biogeosciences 10, 6657–6676, http://dx.doi.org/10.5194/bg-10-6657-2013

Barraza, V., Grings, F., Ferrazzoli, P., Huete, A., Restrepo-Coupe, N., Beringer, J., Van Gorsel, E., Karszenbaum, H., 2014a. Behavior of multitemporal and multisensor passive microwave indices in Southern Hemisphere ecosystems. J. Geophys. Res. Biogeosci. 119, JG002626, http://dx.doi.org/10.1002/2014JG020146

Barraza, V., Grings, F., Ferrazzoli, P., Salvia, M., Maas, M., Rahmoune, R., Vittucci, C., Karszenbaum, H., 2014b. Monitoring vegetation moisture using passive microwave and optical indices in the dry chaco forest, Argentina. IEEE J. Sel. Top. Appl. Earth Obs. Remote Sens. 7, 421–430, http://dx.doi.org/10.1109/JSTARS2013.2268011

Bowman, W.D., 1989. The relationship between leaf water status, gas exchange, and spectral reflectance in cotton leaves. Remote Sens. Environ. 30, 249–255, http://dx.doi.org/10.1016/0034-4257(89) 90066-7

Cleugh, H.A., Leuning, R., Mu, Q., Running, S.W., 2007. Regional evaporation estimates from flux tower and MODIS satellite data. Remote Sens. Environ. 106, 285–304, http://dx.doi.org/10.1016/j.rse.2006.07.007

Cook, B., 2008. Using light-use and production efficiency models to predict photosynthesis and net carbon exchange during forest canopy disturbance. Ecosystems 11, 26–44.

Demarty, J., Chevallier, F., Friend, A.D., Viovy, N., Piao, S., Ciais, P., 2007. Assimilation of global MODIS leaf area index retrievals within a terrestrial biosphere model. Geophys. Res. Lett. 34, L15402, http://dx.doi.org/10.1029/2007GL030014

Dodds, P., Meyer, W.S., Barton, A. 2005. A Review of Methods to Estimate Irrigated Reference Crop Evapotranspiration across Australia (Report No. 04/05).

Ferrazzoli, P., Guerriero, L., 1996. Passive microwave remote sensing of forests: a model investigation. IEEE Trans. Geosci. Remote Sens. 34, 433–443, http://dx.doi.org/10.1109/36.485121

Ferrazzoli, P., Paloscia, S., Pampaloni, P., Schiavon, G., Solimini, D., Coppo, P., 1992. Sensitivity of microwave measurements to vegetation biomass and soil moisture content: a case study. IEEE Trans. Geosci. Remote Sens. 30, 750–756, http://dx.doi.org/10.1109/36.158869

Ferrazzoli, P., Guerriero, L., Paloscia, S., Pampaloni, P., 1995. Modeling X and Ka band emission from Leafy vegetation. J. Electromagn. Waves Appl. 9, 393–406, http://dx.doi.org/10.1163/156939395X00541

Frolking, S., Milliman, T., Palace, M., Wisser, D., Lammers, R., Fahnestock, M., 2005. Tropical forest backscatter anomaly evident in SeaWinds scatterometer morning overpass data during 2005 drought in Amazonia. Remote Sens. Environ. 115, 897–907, http://dx.doi.org/10.1016/j.rse.2010.11.017

Glenn, E.P., Nagler, P.L., Huete, A.R., 2010. Vegetation index methods for estimating evapotranspiration by remote sensing. Surv. Geophys. 31, 531–555, http://dx.doi.org/10.1007/s10712-010-9102-2

Glenn, E.P., Neale, C.M.U., Hunsaker, D.J., Nagler, P.L., 2011. Vegetation index-based crop coefficients to estimate evapotranspiration by remote sensing in agricultural and natural ecosystems. Hydrol. Process. 25, 4050–4062, http://dx.doi.org/10.1002/hyp.8392

Goldstein, G., Andrade, J.L., Meinzer, F.C., Holbrook, N.M., Cavelier, J., Jackson, P., Celis, A., 1998. Stem water storage and diurnal patterns of water use in tropical forest canopy trees. Plant Cell Environ. 21, 397–406, http://dx.doi.org/10.1046/j1365-3040.1998.00273. x

Goldstein, G., Meinzer, F.C., Bucci, S.J., Scholz, F.G., Franco, A.C., Hoffmann, W.A., 2008. Water economy of Neotropical savanna trees: six paradigms revisited. Tree Physiol. 28, 395–404, http://dx.doi.org/10.1093/treephys/28.3.395

Goudriaan, J., 1986. A simple and fast numerical method for the computation of daily totals of crop photosynthesis. Agric. For. Meteorol 38, 249–254, http://dx.doi.org/10.1016/0168-1923(86) 90063-8

Grant, L., 1987. Diffuse and specular characteristics of leaf reflectance. Remote Sens. Environ. 22, 309–322, http://dx.doi.org/10.1016/0034-4257(87) 90064-2

Guerschman, J.P., Van Dijk, A.I.J.M., Mattersdorf, G., Beringer, J., Hutley, L.B., Leuning, R., Pipunic, R.C., Sherman, B.S., 2009. Scaling of potential evapotranspiration with MODIS data reproduces flux observations and catchment water balance observations across Australia. J. Hydrol. 369, 107–119, http://dx.doi.org/10.1016/j.jhydrol.2009.02.013

Hardisky, M.S., 1983. The influence of soil salinity, growth form and leaf moisture on the spectral radiance of Spartina alterniflora canopies. Photogramm. Eng. Remote Sens. 48, 77–84.

Hollinger, D.Y., Aber, J., Dail, B., Davidson, E.A., Goltz, S.M., Hughes, H., Leclerc, M.Y., Lee, J.T., Richardson, A.D., Rodrigues, C., Scott, N.A., Achuatavarier, D., Walsh, J., 2004. Spatial and temporal variability in forest–atmosphere CO_2 exchange. Glob. Change Biol. 10, 1689–1706, http://dx.doi.org/10.1111/j1365-2486.2004.00847. x

Huete, A., Didan, K., Miura, T., Rodriguez, E.P., Gao, X., Ferreira, L.G. 2002. Overview of the radiometric and biophysical performance of the MODIS vegetation indices. Remote Sens. Environ., The Moderate Resolution Imaging Spectroradiometer (MODIS): a new generation of Land Surface Monitoring 83, 195–213. doi:10.1016/S0034-4257(02) 96-2.

Jackson, T.J., 1997. Soil moisture estimation using special satellite microwave/imager satellite data over a grassland region. Water Resour. Res. 33, 1475–1484, http://dx.doi.org/10.1029/97WR00661
Jarvis, P.G., McNaughton, K.G., 1986. Stomatal control of transpiration: scaling up from leaf to region. In: MacFadyen, A., Ford, E.D. (Eds.), Advances in Ecological Research. Academic Press, pp. 1–49.
Jones, M.O., Kimball, J.S., Jones, L.A., McDonald, K.C., 2012. Satellite passive microwave detection of North America start of season. Remote Sens. Environ. 123, 324–333, http://dx.doi.org/10.1016/j.rse.2012.03.025
Jupp, D.L.B., Culvenor, D.S., Lovell, J.L., Newnham, G.J., Strahler, A.H., Woodcock, C.E., 2009. Estimating forest LAI profiles and structural parameters using a ground-based laser called Echidna. Tree Physiol. 29, 171–181, http://dx.doi.org/10.1093/treephys/tpn022
Kalma, J.D., McVicar, T.R., McCabe, M.F., 2008. Estimating land surface evaporation: a review of methods using remotely sensed surface temperature data. Surv. Geophys. 29, 421–469, http://dx.doi.org/10.1007/s10712-008-9037-z
Kawanishi, T., Sezai, T., Ito, Y., Imaoka, K., Takeshima, T., Ishido, Y., Shibata, A., Miura, M., Inahata, H., Spencer, R.W., 2003. The advanced microwave scanning radiometer for the earth observing system (AMSR-E), NASDA's contribution to the EOS for global energy and water cycle studies. IEEE Trans. Geosci. Remote Sens. 41, 184–194, http://dx.doi.org/10.1109/TGRS2002.808331
Kimball, J.S., McDonald, K.C., Zhao, M., 2006. Spring thaw and its effect on terrestrial vegetation productivity in the Western Arctic Observed from satellite microwave and optical remote sensing. Earth Interact. 10, 1–22, http://dx.doi.org/10.1175/EI187.1
Leuning, R., Cleugh, H.A., Zegelin, S.J., Hughes, D., 2005. Carbon and water fluxes over a temperate Eucalyptus forest and a tropical wet/dry savanna in Australia: measurements and comparison with MODIS remote sensing estimates. Agric. For. Meteorol. 129, 151–173, http://dx.doi.org/10.1016/j.agrformet.2004.12.004
Leuning, R., Zhang, Y.Q., Rajaud, A., Cleugh, H., Tu, K., 2008. A simple surface conductance model to estimate regional evaporation using MODIS leaf area index and the Penman–Monteith equation. Water Resour. Res. 44, W10419, http://dx.doi.org/10.1029/2007WR006562
Leuning, R., van Gorsel, E., Massman, W.J., Isaac, P.R., 2012. Reflections on the surface energy imbalance problem. Agric. For. Meteorol. 156, 65–74, http://dx.doi.org/10.1016/j.agrformet.2011.12.002
Li, R., Min, Q., Lin, B., 2009. Estimation of evapotranspiration in a mid-latitude forest using the microwave emissivity difference vegetation index (EDVI). Remote Sens. Environ. 113, 2011–2018, http://dx.doi.org/10.1016/j.rse.2009.05.007
Matsumoto, K., Ohta, T., Tanaka, T., 2005. Dependence of stomatal conductance on leaf chlorophyll concentration and meteorological variables. Agric. For. Meteorol 132, 44–57, http://dx.doi.org/10.1016/j.agrformet.2005.07.001
Meyer, W.S., Wayne S. 1999. Standard reference evaporation calculation for inland, south eastern Australia [electronic resource]/by Wayne S. Meyer, PANDORA electronic collection., Technical report (CSIRO. Land and Water: Online); no. 98/35. CSIRO Land and Water, [Canberra].
Meyers, T., Baldocchi, D., 2005. Current Micrometeorological Flux Methodologies with Applications in Agriculture. Publ. Agencies Staff US Dep. Commer.
Min, Q., Lin, B., 2006. Remote sensing of evapotranspiration and carbon uptake at Harvard Forest. Remote Sens. Environ. 100, 379–387, http://dx.doi.org/10.1016/j.rse.2005.10.020
Moncrieff, J.b., Malhi, Y., Leuning, R., 1996. The propagation of errors in long-term measurements of land-atmosphere fluxes of carbon and water. Glob. Change Biol. 2, 231–240, http://dx.doi.org/10.1111/j1365-2486.1996.tb00075.x
Monteith, J.L., 1985. Evaporation from land surfaces: progress in analysis and prediction since 1948. Advances in Evapotranspiration. Presented at the Proceedings of the ASAE Conference on Evapotranspiration 985, 4–12.
Moran, M.S., Jackson, R.D., 1991. Assessing the spatial distribution of evapotranspiration using remotely sensed inputs. J. Environ. Qual. 20, 725, http://dx.doi.org/10.2134/jeq1991.00472425002000040003x
Mu, Q., Zhao, M., Running, S.W., 2011. Improvements to a MODIS global terrestrial evapotranspiration algorithm. Remote Sens. Environ. 115, 1781–1800, http://dx.doi.org/10.1016/j.rse.2011.02.019
Mu, Q., 2007. Development of a global evapotranspiration algorithm based on MODIS and global meteorology data. Remote Sens. Environ. 111, 519–536, http://dx.doi.org/10.1016/j.rse.2007.04.015
Paloscia, S., Pampaloni, P., 1988. Microwave polarization index for monitoring vegetation growth. IEEE Trans. Geosci. Remote Sens. 26, 617–621, http://dx.doi.org/10.1109/36.7687
Paloscia, S., Pampaloni, P., 1992. Microwave vegetation indexes for detecting biomass and water conditions of agricultural crops. Remote Sens. Environ. 40, 15–26, http://dx.doi.org/10.1016/0034-4257(92)90123-2
Pfautsch, S., Bleby, T.M., Rennenberg, H., Adams, M.A., 2010. Sap flow measurements reveal influence of temperature and stand structure on water use of Eucalyptus regnans forests. For. Ecol. Manage. 259, 1190–1199, http://dx.doi.org/10.1016/j.foreco.2010.01.006
Pipunic, R.C., Walker, J.P., Western, A.W., Trudinger, C.M., 2013. Assimilation of multiple data types for improved heat flux prediction: a one-dimensional field study. Remote Sens. Environ. 136, 315–329, http://dx.doi.org/10.1016/j.rse.2013.05.015
Restrepo-Coupe, N., da Rocha, H.R., Hutyra, L.R., da Araujo, A.C., Borma, L.S., Christoffersen, B., Cabral, O.M.R., de Camargo, P.B., Cardoso, F.L., da Costa, A.C.L., Fitzjarrald, D.R., Goulden, M.L., Kruijt, B., Maia, J.M.F., Malhi, Y.S., Manzi, A.O., Miller, S.D., Nobre, A.D., von Randow Sá, L.D.A., Tota, J., Wofsy, S.C., Zanchi, F.B., Saleska, S.R., 2013. What drives the seasonality of photosynthesis across the Amazon basin? A cross-site analysis of eddy flux tower measurements from the Brasil flux network. Agric. For. Meteorol. 182–183, 128–144, http://dx.doi.org/10.1016/j.agrformet.2013.04.031
Richardson, A.D., Hollinger, D.Y., Burba, G.G., Davis, K.J., Flanagan, L.B., Katul, G.G., William Munger, J., Ricciuto, D.M., Stoy, P.C., Suyker, A.E., Verma, S.B., Wofsy, S.C., 2006. A multi-site analysis of random error in tower-based measurements of carbon and energy fluxes. Agric. For. Meteorol. 136, 1–18, http://dx.doi.org/10.1016/j.agrformet.2006.01.007
Schmid, H.P., Grimmond, C.S.B., Cropley, F., Offerle, B., Su, H.-B., 2000. Measurements of CO2 and energy fluxes over a mixed hardwood forest in the mid-western United States. Agric. For. Meteorol 103, 357–374, http://dx.doi.org/10.1016/S0168-1923(00)140-4
Strahler, A.H., Jupp, D.L., Woodcock, C.E., Schaaf, C.B., Yao, T., Zhao, F., Yang, X., Lovell, J., Culvenor, D., Newnham, G., Ni-Miester, W., Boykin-Morris, W., 2008. Retrieval of forest structural parameters using a ground-based lidar instrument (Echidna®). Can. J. Remote Sens. 34, S426–S440, http://dx.doi.org/10.5589/m08-046
Urbanski, S., Barford, C., Wofsy, S., Kucharik, C., Pyle, E., Budney, J., McKain, K., Fitzjarrald, D., Czikowsky, M., Munger, J.W., 2007. Factors controlling CO_2 exchange on timescales from hourly to decadal at Harvard Forest. J. Geophys. Res. Biogeosci. 112, G02020, http://dx.doi.org/10.1029/2006JG000293
Wilson, K., Goldstein, A., Falge, E., Aubinet, M., Baldocchi, D., Berbigier, P., Bernhofer, C., Ceulemans, R., Dolman, H., Field, C., Grelle, A., Ibrom, A., Law, B.E., Kowalski, A., Meyers, T., Moncrieff, J., Monson, R., Oechel, W., Tenhunen, J., Valentini, R., Verma, S., 2002. Energy balance closure at FLUXNET sites. Agric. For. Meteorol. FLUXNET 2000 Synth. 113, 223–243, http://dx.doi.org/10.1016/S0168-1923(02)109-0
Yebra, M., Van Dijk, A., Leuning, R., Huete, A., Guerschman, J.P., 2013. Evaluation of optical remote sensing to estimate actual evapotranspiration and canopy conductance. Remote Sens. Environ. 129, 250–261, http://dx.doi.org/10.1016/j.rse.2012.11.004
Zhang, Y.-J., Meinzer, F.C., Qi, J.-H., Goldstein, G., Cao, K.-F., 2013. Midday stomatal conductance is more related to stem rather than leaf water status in subtropical deciduous and evergreen broadleaf trees. Plant Cell Environ. 36, 149–158, http://dx.doi.org/10.1111/j1365-3040.2012.02563. x.